THE 5th INTERNATIONAL CONFERENCE
MECHANICAL ENGINEERING IN XXI CENTURY

December 9-10, 2020
Faculty of Mechanical Engineering in Niš, Serbia

Bucket Wheel Excavators: Balancing and Dynamic Response of the Slewing Superstructure

Srđan BOŠNJAK, Nebojša GNJATOVIĆ

First Author affiliation: University of Belgrade-Faculty of Mechanical Engineering, Kraljice Marije 16, Belgrade, Serbia
Second Author affiliation: University of Belgrade-Faculty of Mechanical Engineering, Kraljice Marije 16, Belgrade, Serbia
sbosnjak@mas.bg.ac.rs; ngnjatovic@mas.bg.ac.rs

***Abstract*—A slewing superstructure (SS) represents a key functional subsystem of bucket wheel excavators (BWEs). Identification of its basic parameters of static stability (BPSS: weight and position of the center of gravity) is of equally crucial significance in design of a BWE and in its exploitation. The BPSS dominantly determine the static stability of a BWE SS and, coupled with stiffness, its dynamic response. This paper presents the results of research on the impact of the difference between the experimentally and analytically determined SS BPSS on the: (1) intensities of forces in the ropes of the bucket wheel boom hoisting mechanism; (2) maximum loads of the SS radiaxial slew bearing balls; (3) dynamic response of the SS. The presented research represents the initial stage in forming of the integral methodology for the assessment of impact of the mentioned differences on the key indicators which determine the lifespan and integrity, as well as reliability and safety of the SS of BWEs and related surface mining and material handling machines.**

***Keywords*—Bucket Wheel Excavator, Slewing Superstructure, Weighing, Balancing, Dynamic Response**

I. INTRODUCTION

Thermal power plants hold the biggest share of the energy production in Serbia. According to [1], [2] roughly 70% of electricity produced in Serbia comes from lignite. In Europe, only Germany and Turkey hold bigger reserves of lignite than Serbia, meaning that lignite will remain the primary energetic potential of Serbia for the foreseeable future [1], [3]. Serbian lignite reserves are large enough to support the projected energy consumption until the end of the 21st century [3].

The backbone of lignite production lies in the surface mining systems (SMSs), which are regarded as one of the most significant achievements in the field of mining in the 20th century [4], [5]. The heart of any such system is a bucket wheel excavator (BWE), which dominantly determines its performance, first and foremost reflected on its capacity.

BWEs, the biggest self-propelled machines in existence [6], are exploited in harsh working conditions (24/7) [7], in which they are exposed to the loads of a pronounced dynamic and stochastic character [8]–[11]. Downtimes in their operation adversely affect the coal production and consequently lead to very high direct and/or indirect expenses [5], [12], [13].

A slewing superstructure (SS) represents a vital functional subsystem of a BWE. Due to its large size and mass, changeable geometric configuration and complex loading conditions, a SS has a dominant impact on the static stability of the machine. Furthermore, relatively small stiffness of the SS substructures combined with, from the dynamic behavior standpoint, unfavorable distribution of relatively large masses, makes it sensitive to the action of periodic excitation caused by the resistance to excavation.

Static stability of the SS is determined by its so called 'basic parameters of static stability' (BPSS) [14]: the weight and position of the center of gravity (CoG). Furthermore, balancing of the SS affects the: (a) integrity and lifespan of the large scale radiaxial slew bearing (RSB) [20], [21] and the vital elements of the structure of, for example, the bucket wheel boom (BWB) stays [23]; (b) dynamic characteristics and response [24]–[32]. For this reason, the SS weight and CoG position are, immediately upon the first erection, determined experimentally by the so called 'weighing' [15]–[19]. Assessing the impact of the unavoidable difference between the experimentally and analytically determined BPSS represents a serious engineering challenge because this problem is, in authors' opinion, unacceptably marginalized in the referent literature and technical regulations. Only the paper [33] presents a method for forming the analytical model for the proof of static stability of the SS, based on the difference between the experimentally and analytically determined BPSS. It is for this reason that the basic analysis of the impact of said difference on the definitive counterweight (CW) mass, loading of the RSB and the dynamic response of the SS is presented in this paper, on the example of the BWE SchRs 1600, Fig. 1. A spatial reduced dynamic model of the SS, developed in [34] based on the procedure presented in [35] and [36], is used in papers [37] and [38] for the analysis of the impact of mass of the CW and mass of the adhered material on the response of the SS. Using a planar dynamic model formed on the basis of procedures presented in [35] and [36], the paper [39] analyzes the impact of mass of the bucket wheel with drive on the

dynamic response of the SS. However, the research presented in papers [37]–[39] were not focused on the explicit analysis of the impact of change in the position of the SS CoG, inevitably caused by the variation in the masses of the CW, the adhered material and the bucket wheel with drive. Therefore, the research presented in this paper present the initial stage in the development of an integral methodology for the assessment of the impact of the difference between the experimentally and analytically determined BPSS on the key indicators which determine the integrity and lifespan, and the reliability and safety of the SSs of BWEs and related surface mining and material handling machines.

Fig. 1 BWE SchRs 1600 in the open pit mine "Tamnava West Field"-Serbia (total mass 2420 t)

II. Balancing of the Slewing Superstructure

Changeability of the position of the SS CoG is the consequence of change in the BWB inclination angle. In the case of BWE SchRs 1600, this angle varies between α_{BWB}==–19.52° (BWB in low position) and α_{BWB}=14.1° (BWB in high position). Identification of BPSS of the designed slewing superstructure of the BWE SchRs 1600, Figs. 2 and 3, as well as mass of the CW for balancing of its deadweight, Fig. 4, was achieved using an analytical model based on the 3D model created from the technical documentation [40] provided by the manufacturer (Krupp), Table I. Such analytical model (model 1: M1) represents the designed image of the slewing superstructure i.e. it's so called 'a priori' model [33].

According to [41], the mass of the CW needed for balancing of the superstructure deadweight in horizontal position (H) of the BWB ($x_{CoG,H,M1}$=0) is $m_{CW,0,H,F}$=177.5 t. For this reason, the first weighing (W1) of the SS was performed with CW mass of $m_{CW,W1}$=177.017 t, Table II [42]. The BPSS of the SS model M1 for the CW mass $m_{CW,W1}$ are presented in Table III.

The averaged mass of the SS established from the results of W1 was determined from the expression

$$m_{SS,0,M1,W1,A} = \frac{\sum_p G_{SS,W1,p}}{3g} - m_{CW,W1} =$$

$$= \frac{11499.2 + 11501.1 + 11494.4}{3 \times 9.81} - 177.017 = 995.246 \text{ t}, \quad (1)$$

where p is the indicator of the BWB measuring position: L, H, Hi, Table II. The difference between the experimentally determined and the designed mass of the SS, model M1, Table I, is

$$m_{cor} = m_{SS,0,M1,W1,A} - m_{SS,0,M1} =$$
$$= 995.246 - 978.266 = 16.98 \text{ t} \quad (2)$$

is in the paper [14] labeled as corrective mass. The procedure for determining the coordinates of its center of mass relative to the local coordinate system of the BWB is presented in [14], while the Table IV showcases the values of said coordinates relative to the coordinate system *Oxyz*, Fig. 2. By introducing the corrective mass into the SS model M1 a real image (present state) of the SS i.e. a so called 'a posteriori' model [33], M2, was formed, Tables V and VI. Impacts of the corrective mass on the SS CoG abscissas' values and the intensities of the BWB hoisting mechanism ropes are presented in Figs. 5 and 6. Upon the correction of the CW mass (Δm_{CW}=54.96 t added [43], [44]), a control weighing was conducted (W2), Fig 7, in which the BWB was in the low position, at the angle α_{BWB}=–11.4° [44]. Therefore, the excavator was deployed with the CW mass of

$$m_{CW,E} = m_{CW,W2} = m_{CW,W1} + \Delta m_{CW} =$$

$$= 177.017 + 54.96 = 231.977 \text{ t}.$$

in place of the designed CW mass of $m_{CW,D,P}$=197 t [45], or, $m_{CW,D,F}$=221 t according to [41]. The impacts of the CW mass in the domain of its variation from $m_{CW,D,P}$=197 t to $m_{CW,E}$=231.977 t on the total masses of the SS models M1 and M2 as well as the calculated CoG abscissas are given in Figs. 8 and 9, respectively.

After determining the definitive mass of the CW, the next step in the examination of the SS balancing is to analyze the position of the point where the vertical component of the principal load vector intersects the referent plane of the RSB (point A), under the effects of the main operating loads: the SS deadweight ($E=m_{SS}g$), the weight of the transported material (F_1) and the incrustation (V_1) on the BWB conveyor (the so called 'conveyor 1'), the weight of the incrustation on the BW (V_0), the tangential (U) and the lateral (S) component of cutting force. The intensities of the non-permanently acting loads (F_1, V_1, V_0, U_F, U_L, S_F and S_L), listed in Table VII, are determined in accordance to the standard [46]. For the assessment of the position of the point A on the BW side, the horizontal position of the BWB is representative, while the high position of the BWB is referent for assessing the said position on the side of the CW. The coordinates of the principal vector and the principal moment of the SS load, referent for determining the position of the point A, are calculated with the expressions

$$Z = \sum_i Z_i,$$

$$M_x = \sum_i \left(Z_i y_i - Y_i z_i \right),$$

$$M_y = \sum_i \left(X_i z_i - Z_i x_i \right),$$

where i=E, F_1, V_0, V_1, U_F and S_F for the BW side i.e. i=E,U_L and S_L for the CW side. Coordinates of the point A are determined with the expressions

$$x_A = -\frac{M_y}{Z},$$

$$y_{\mathrm{A}} = \frac{M_{\mathrm{x}}}{Z}.$$

Based on the eccentricity of the vertical coordinate of the principal vector (e_{Z}) to the center of mass of the RSB,

$$e_{\mathrm{Z}} = \sqrt{x_{\mathrm{A}}^2 + y_{\mathrm{A}}^2},$$

its relative eccentricity is determined

$$e_{\mathrm{r}} = \frac{e_{\mathrm{Z}}}{D_{\mathrm{RSB}}},$$

Fig. 10, where D_{RSB}=11 m is the race diameter of the RSB. Having in mind the fact that the relative eccentricity was determined for the set of loads acting during normal operation of the machine (in relation to the load case H1.1 [46] only the impact of the inclination was omitted), it is necessary to determine if the vertical component of the principal vector is acting within the core of the supporting contour cross section (a circle with the radius of e=0.25D_{RSB}), i.e. to meet the condition

$$e_{\mathrm{r}} < 0.25, \tag{3}$$

which ensures that the load is distributed across all the balls of the RSB. The maximum load of a RSB ball is determined according to the expression [15]

$$F_{\mathrm{B,max}} = \frac{|Z|}{n_{\mathrm{B}}}\left(1 + 4e_{\mathrm{r}}\right),$$

Fig. 11, where n_{B}=141 is the total number of balls in the considered RSB.

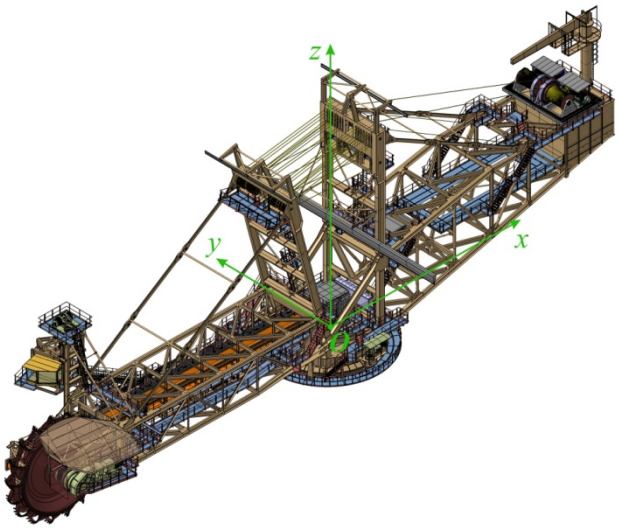

Fig. 2 Slewing superstructure of the BWE SchRs 1600 (total mass without counterweight: $m_{\mathrm{SS,0,M1}}$=978.266 t; *Oxyz*-coordinate system related to the center of the RSB)

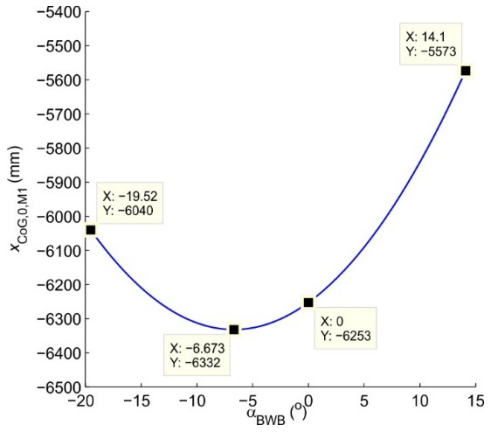

Fig. 3 Abscissa (x_{CoG}) of the SS model M1 CoG (without CW)

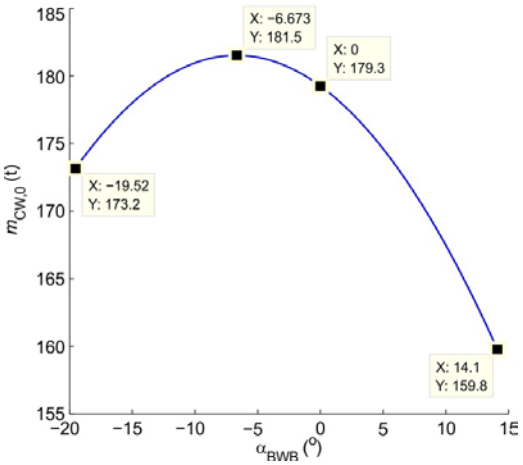

Fig. 4 Mass of the CW ($m_{\mathrm{CW,0}}$) for balancing the SS model M1 deadweight

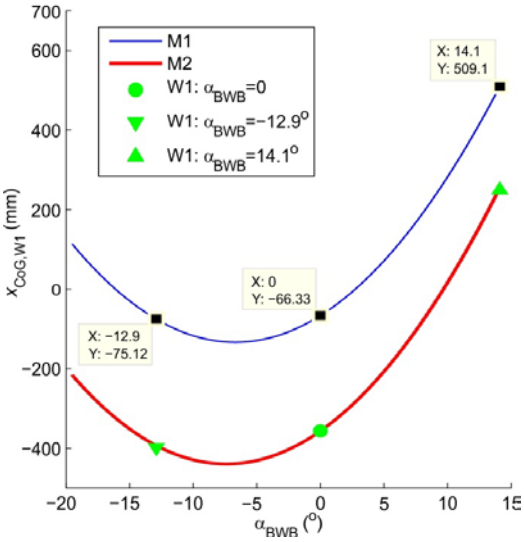

Fig. 5 Calculation CoG abscissas of the SS models M1 and M2 (with CW mass $m_{\mathrm{CW,W1}}$=177.017 t) vs. experimentally determined CoG abscissa (W1)

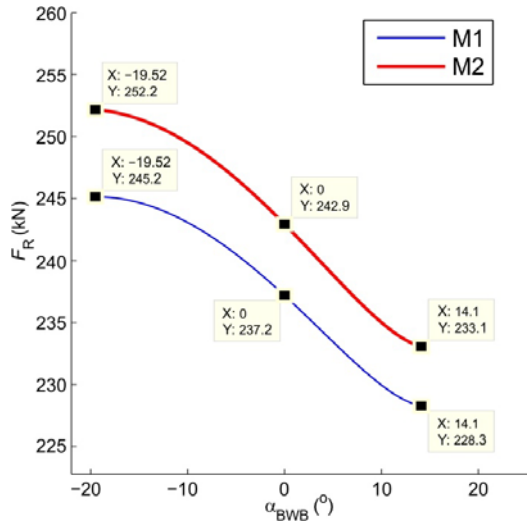

Fig. 6 Winch rope forces caused by the deadweight: M1 vs. M2

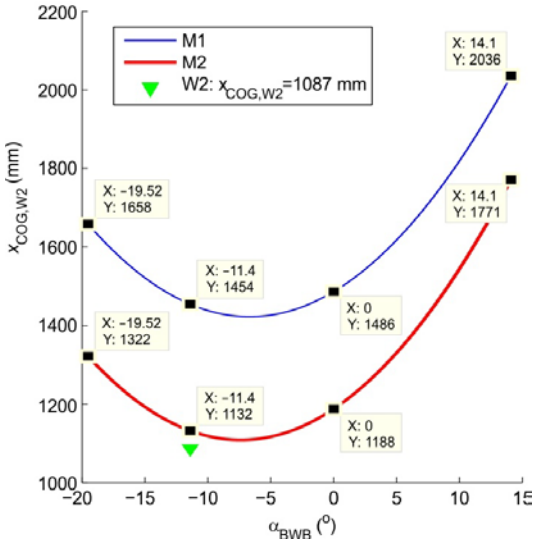

Fig. 7 Calculation CoG abscissas of the SS models M1 and M2 (with CW mass $m_{CW,W2}$=231.977 t) vs. experimentally determined CoG abscissa (W2)

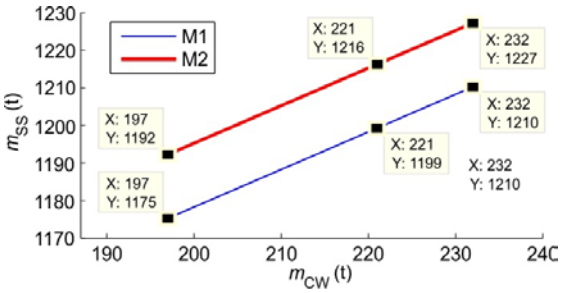

Fig. 8 Impact of the CW mass on the SS models M1 and M2 total mass

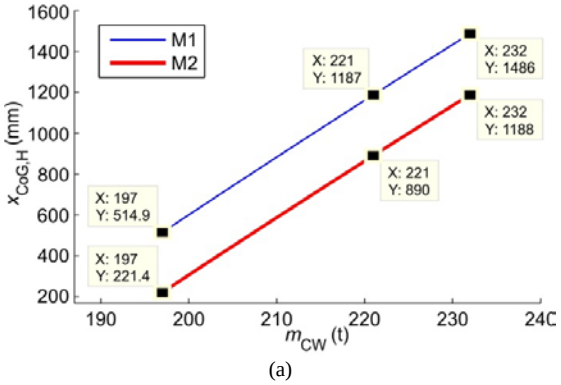

(a)

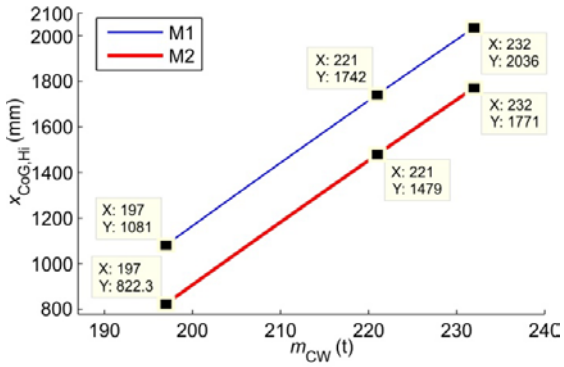

(b)

Fig. 9 Impact of the CW mass on calculation CoG abscissas of the SS models M1 and M2 for BWB position H (a) and Hi (b)

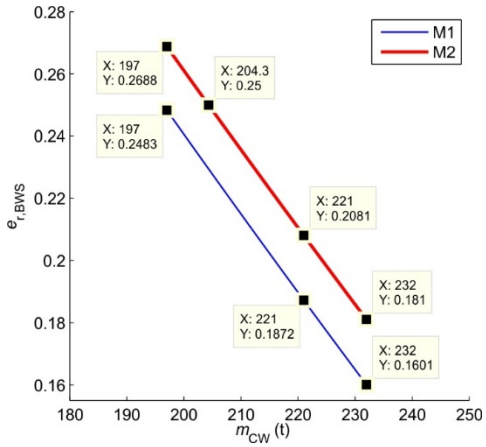

(a)

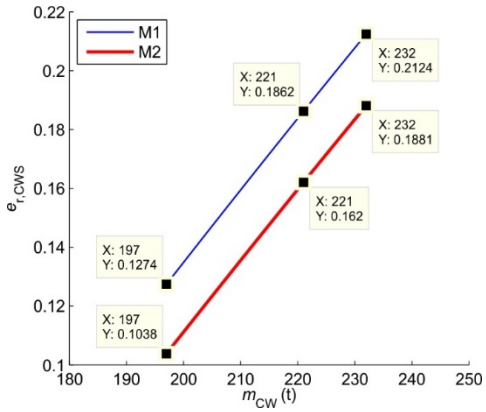

(b)

Fig. 10 Impact of the CW mass on the relative RSB vertical load eccentricity on the BW side (a) and CW side (b)

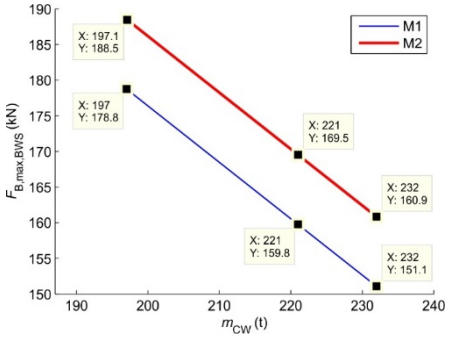

(a)

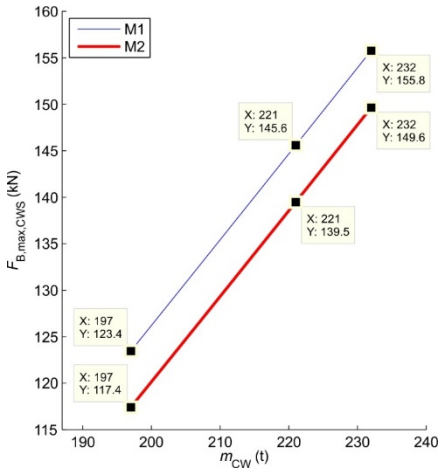

(b)

Fig. 11 Impact of the CW mass on the RSB balls' maximum load

TABLE I BPSS OF THE SS MODEL M1 (WITHOUT COUNTERWEIGHT)

Nomenclature	Notation	Value
Mass	$m_{SS,0,M1}$	978.266 t
CoG abscissa	$x_{CoG,0,M1}$	–6253 mm (α_{BWB}=0)
		–5573 mm (α_{BWB}=14.1°)
		–6040 mm (α_{BWB}=–19.52°)
CoG ordinate	$y_{CoG,0,M1}$	–154 mm

TABLE II RESULTS OF THE FIRST SS WEIGHING (W1)

BWB measuring position	Weight* (kN)	CoG position (mm)	
	$G_{SS,W1}$	$x_{CoG,W1}$	$y_{CoG,W1}$
Low (L): α_{BWB}=–12.9°	11499.2	–398	–121
Horizontal (H): α_{BWB}=0	11501.1	–356	–125
High (Hi): α_{BWB}=14.1	11499.4	249	–118

*counterweight mass: $m_{CW,W1}$=177.017 t

TABLE III CALCULATED BPSS OF THE SS MODEL M1 FROM W1

BWB measuring position	Mass* (t)	CoG position (mm)	
	$m_{SS,W1,M1}$	$x_{CoG,W1,M1}$	$y_{CoG,W1,M1}$
Low (L): α_{BWB}=–12.9°	1155.283	–75	–130
Horizontal (H): α_{BWB}=0		–66	
High (Hi): α_{BWB}=14.1		509	

*counterweight mass: $m_{CW,W1}$=177.017 t

TABLE IV POSITION OF THE CORRECTIVE MASS CENTER (CMC)

BWB measuring position	CMC coordinates (mm)		
	x_{CMC}	y_{CMC}	z_{CMC}
Low (L): α_{BWB}=–12.9°	–22001	475	6511
Horizontal (H): α_{BWB}=0	–20090		14068
High (Hi): α_{BWB}=14.1	–17070		17704

TABLE V BPSS OF THE SS MODEL M2 (WITHOUT COUNTERWEIGHT)

Nomenclature	Notation	Value
Mass	$m_{SS,0,M2}$	995.246 t
CoG abscissa	$x_{CoG,0,M2}$	–6489 mm (α_{BWB}=0)
		–5769 mm (α_{BWB}=14.1°)
		–6323 mm (α_{BWB}=–19.52°)
CoG ordinate	$y_{CoG,0,M2}$	–143 mm

TABLE VI CALCULATION BPSS OF THE SS MODEL M2 FROM W1

BWB measuring position	Mass* (t)	CoG position (mm)	
	$m_{SS,W1,M2}$	$x_{CoG,W1,M2}$	$y_{CoG,W1,M2}$
Low (L): α_{BWB}=–12.9°	1172.263	–393	–121
Horizontal (H): α_{BWB}=0		–356	
High (Hi): α_{BWB}=14.1		–255	

*counterweight mass: $m_{CW,W1}$=177.017 t

TABLE VII INTENSITIES AND POSITIONS OF THE LOADS

Load	Intensity (kN)	Position of points of application		
		x (m)	y (m)	z (m)
BWB position: H				
F_1	376.1	–22.078	0.85	4.475
V_1	37.6	–22.078	0.85	4.475
V_0	196.6	–40.166	–0.76	3.675
U_F	505.1	–46.291	–0.12	4.035
S_F	204.4	–46.291	–0.12	4.035
BWB position: Hi				
U_L	505.1	–38.985	–0.12	6.74
S_L	235.5	–38.985	–0.12	6.74

III. DYNAMIC RESPONSE OF THE SLEWING SUPERSTRUCTURE

The analysis of the influence of the CW mass on the modal characteristics and the dynamic response of the SS was conducted using reduced spatial dynamic models M1 ('a priori' model) and M2 ('a posteriori' model) of the SS, developed according to the procedure presented in detail in [34], Fig. 12. Dynamic models formed in this manner enable the analysis of the BWE SS dynamic behavior in the conditions of continuous variation of both the constructional parameters and the parameters of excitation. BWB inclination angle, as proven in [47], does not have a significant impact on the modal characteristics of the analyzed SS of the BWE SchRs 1600, which is the consequence of a relatively small length and extension of the ropes of the BWB hoisting mechanism, thus the horizontal position of the BWB was adopted as referent for further analysis.

Under the assumption that the excavating angle is equal to $\psi_E=\pi/2$ and having in mind the fact that the appearance of parametric oscillations has not been observed during the exploitation of the excavator [37], identification of the external loads caused by the resistance to excavation was performed according to the procedures presented in [48], [49]. Available moment of excavation was determined according to the equation,

$$M_{E,av}=\frac{\eta_{BWD}P_{BWD}-P_h}{\omega_{BW}}, \quad (4)$$

where η_{BWD}=0.9 is the efficiency of the BW drivetrain, P_{BWD}=1150 kW is BW drive power and P_h is the power used to lift the material in the BW obtained from the expression:

$$P_h = Q_{th}\rho_o g h_Q. \quad (5)$$

In the expression (5), Q_{th}=6600 m^3/h represents the theoretical capacity of the machine, ρ_o=1700 kg/m^3 is the mass density of the overburden (loose), g=9.81 m/s^2 is the gravity constant, while h_Q=D_{BW}/2=12.25/2=6.125 m is the material lifting height [15]. Angular frequency of the BW is calculated using the equation,

$$\omega_{BW} = \frac{n_D 2\pi}{n_B}, \quad (6)$$

where n_D=69.4 min^{-1} is the frequency of bucket discharge, while n_B=17 represents the number of buckets.

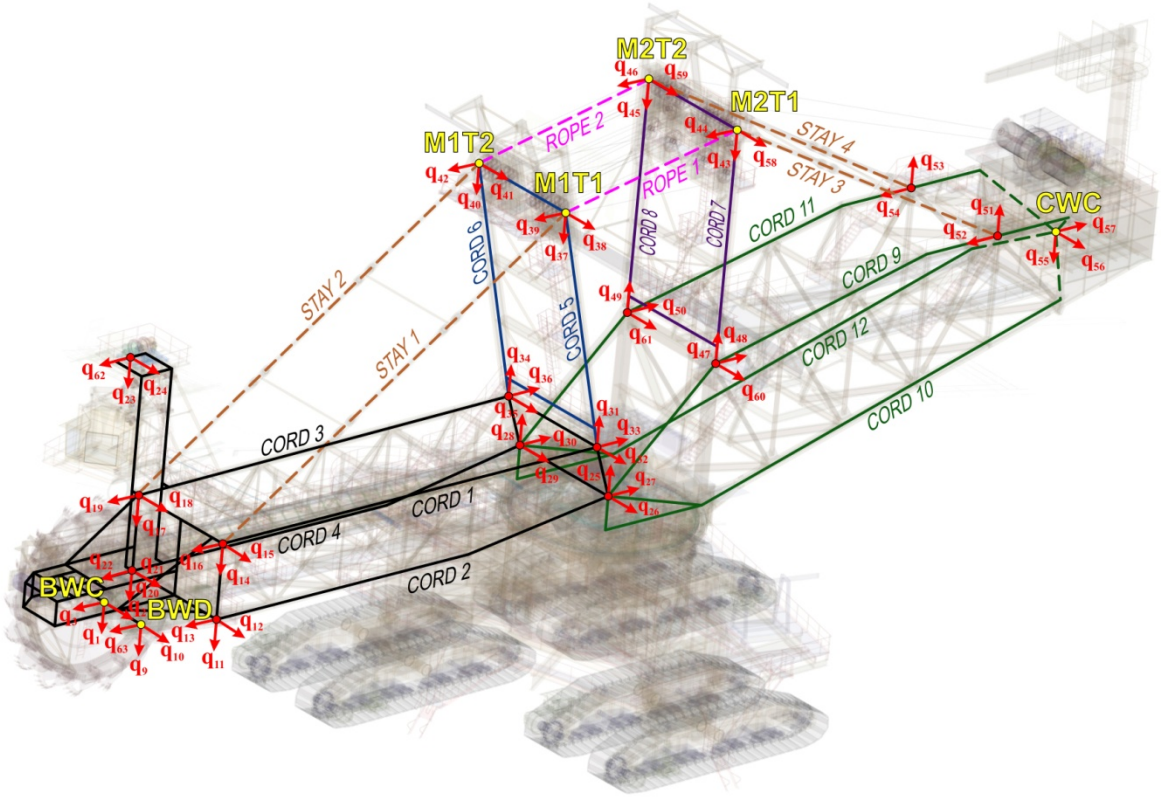

Fig. 12 Spatial reduced dynamic model of the BWE SchRs 1600 superstructure (extracted from Fig. 2 in [47])

If the maximum moment of excavation ($M_{E,max}$), occurring when the maximum number of buckets are engaged in the cut ($n_{B,E,max}$=$n_{B,E,min}$+1), is calculated according to the expression,

$$M_{E,max} = \frac{D_{BW}}{2} k_F s_0 b_0 \sum_{i=0}^{n_{B,E,min}} \sin(\psi_E - i\theta_B) = M_{E,av}, \quad (7)$$

then the expression (7) yields to

$$k_F s_0 b_0 = \frac{2M_{E,av}}{D_{BW} \sum_{i=0}^{n_{B,E,min}} \sin(\psi_E - i\theta_B)}, \quad (8)$$

allowing the calculation of the minimum moment of excavation ($M_{E,min}$) occurring when the minimum number of buckets are engaged in the cut ($n_{B,E,min}$=int(ψ_E/θ_B)):

$$M_{E,min} = \frac{M_{E,av}}{\sum_{i=0}^{n_{B,E,min}} \sin(\psi_E - i\theta_B)} \sum_{i=1}^{n_{B,E,min}} \sin(\psi_E - i\theta_B), \quad (9)$$

where θ_B=2π/n_B is the angular step of the buckets. The obtained external loads, caused by the resistance to excavation, were approximated with trigonometric polynomials with n=5 harmonics, using the Fourier coefficients, as indicated in [37]. The trigonometric polynomial of the excavation moment ($M_{E,F}$(t)), Fig. 13, was formed according to the equation,

$$M_{E,F}(t) = \frac{M_{E,max} + M_{E,min}}{2} + \sum_{n=1}^{5} \frac{M_{E,min} - M_{E,max}}{n\pi} \sin(n\Omega t), \quad (10)$$

where Ω=2πn_D is the fundamental angular frequency of excitation.

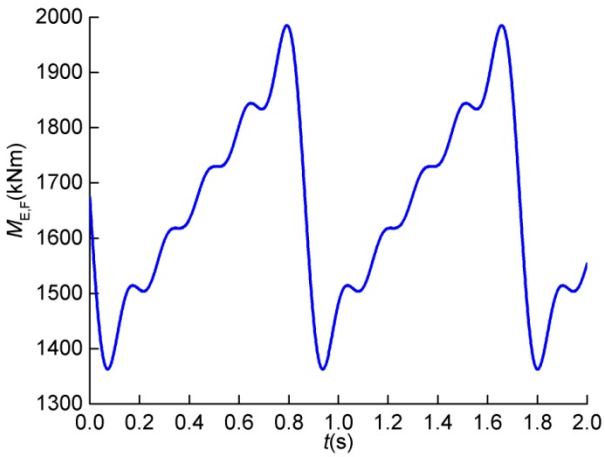

Fig. 13 Moment of excavation $M_{E,F}$(t)

The forced responses of the dynamic models M1 and M2 were determined by applying the Lagrange's second order equations, under the assumption that the structural damping may be considered negligible in the out-of-resonance region, while also having in mind the fact that

free vibration responses are quickly attenuated in operation.

Under the previous assumptions, the system of differential equations of motion yields to [37]

$$\mathbf{M}(m_{\mathrm{CW}})\cdot\ddot{\mathbf{q}}(m_{\mathrm{CW}},t)+\mathbf{K}\cdot\mathbf{q}(m_{\mathrm{CW}},t)= \\ =\mathbf{Q}_{\Omega}^{\mathbf{0}}+\sum_{n=1}^{5}\mathbf{Q}_{\Omega}^{\mathbf{n}}\sin(n\Omega t). \tag{11}$$

It is important to note that the mass matrix of the system $\mathbf{M}(m_{\mathrm{CW}})$ is dependent on the CW mass, ranging from $m_{\mathrm{CW,D,P}}$=197 t to $m_{\mathrm{CW,E}}$=231.977 t ≈232 t, which makes the generalized displacements,

$$\mathbf{q}(m_{\mathrm{CW}},t)=\mathbf{A}_{\mathbf{0}}+\sum_{n=1}^{5}\mathbf{A}_{\mathbf{n}}(m_{\mathrm{CW}})\sin(n\Omega t), \tag{12}$$

and accelerations of the system referent points,

$$\mathbf{a}(m_{\mathrm{CW}},t)=-\sum_{n=1}^{5}n^{2}\Omega^{2}\mathbf{A}_{\mathbf{n}}(m_{\mathrm{CW}})\sin(n\Omega t), \tag{13}$$

dependent on the CW mass in addition to time.

The spectrum of natural frequencies of the model was adopted in a way that accounts for the first five frequencies of excitation [37], while the transformation from M1 to M2 model was realized with the inclusion of the corrective mass (m_{cor}) as a lumped mass with coordinates enclosed in Table IV.

Modal characteristics of both analyzed models (M1 and M2) in the conditions of continuous CW mass variation are presented in Fig. 14, while the values of first 13 natural frequencies obtained for the initial and ultimate values of parameter range are enclosed in Table VIII.

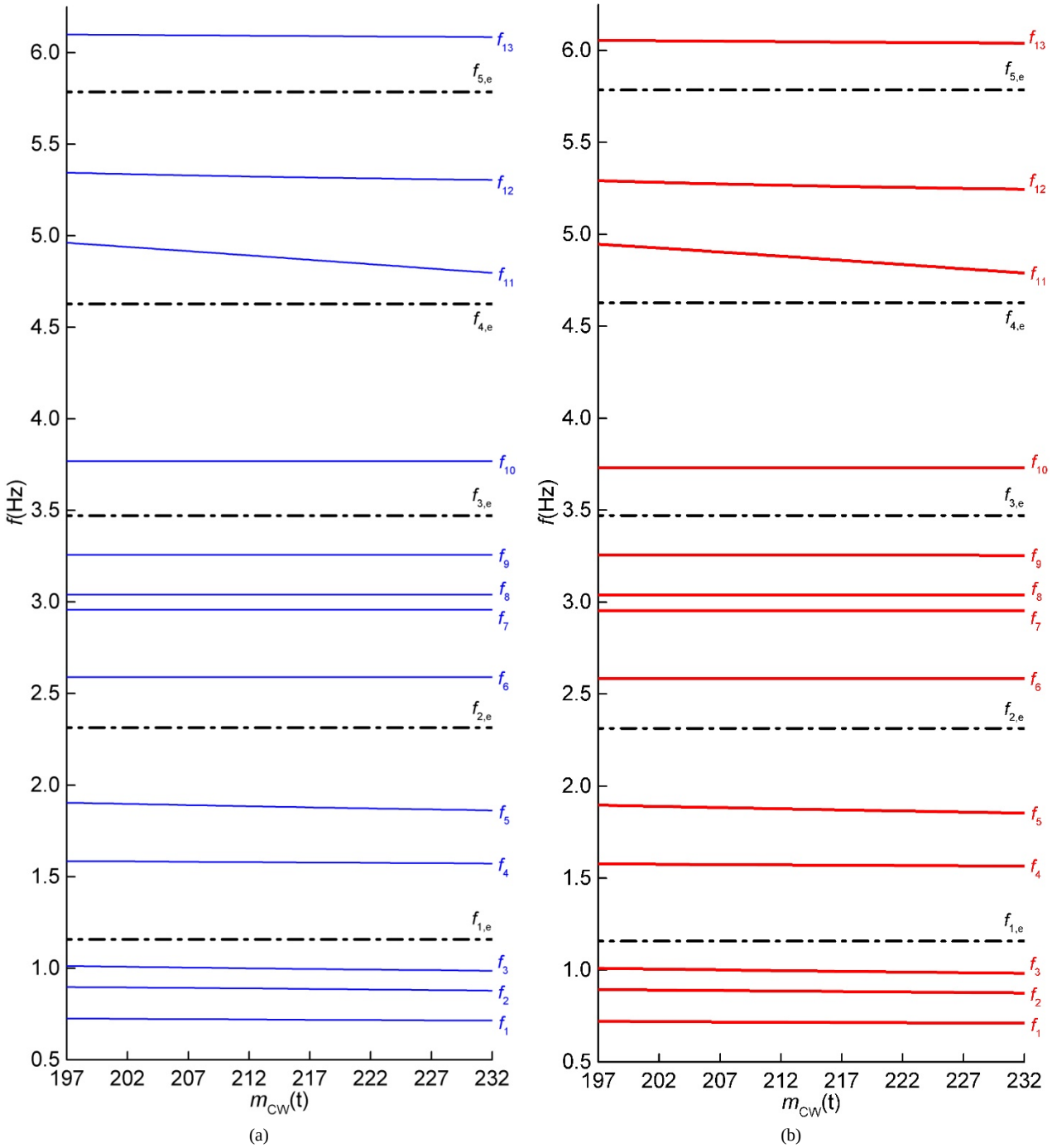

Fig. 14 Dependence of natural frequencies on the CW mass: (a) model M1; (b) model M2 (free vibration frequencies of M1 - blue continuous lines;

free vibration frequencies of M2 - red continuous lines; forced vibration frequencies - black dash-dot lines)

TABLE VIII INFLUENCE OF THE CW MASS ON THE SPECTRUM OF NATURAL FREQUENCIES – MODELS M1 & M2

Model	m_{CW}	Natural frequency (Hz)												
		f_1	f_2	f_3	f_4	f_5	f_6	f_7	f_8	f_9	f_{10}	f_{11}	f_{12}	f_{13}
M1	$m_{CW,D,P}$	0.725	0.897	1.012	1.585	1.904	2.589	2.957	3.039	3.257	3.768	4.961	5.344	6.098
	$m_{CW,E}$	0.714	0.877	0.986	1.571	1.861	2.589	2.957	3.039	3.257	3.768	4.797	5.304	6.084
M2	$m_{CW,D,P}$	0.721	0.893	1.01	1.577	1.897	2.586	2.954	3.039	3.255	3.730	4.946	5.291	6.055
	$m_{CW,E}$	0.711	0.875	0.983	1.565	1.853	2.586	2.954	3.039	3.254	3.730	4.789	5.245	6.039

Analysis of the dynamic response was conducted by monitoring the generalized vertical and lateral displacements and accelerations of the referent points of the system which are most sensitive to the variation of the constructional parameters [7], [32], [39], [47]. Maximum generalized displacements of: (a) bucket wheel center – BWC; (b) bucket wheel drive gearbox center of gravity – BWD; (c) tips of the mast 1 – M1T1 and M1T2; (d) tips of the mast 2 – M2T1 and M2T2; (e) counterweight center of gravity – CWC, Fig. 12, are presented in Figs. 15-26, while the maximum vertical and lateral accelerations of these referent points are enclosed in Figs. 27-38.

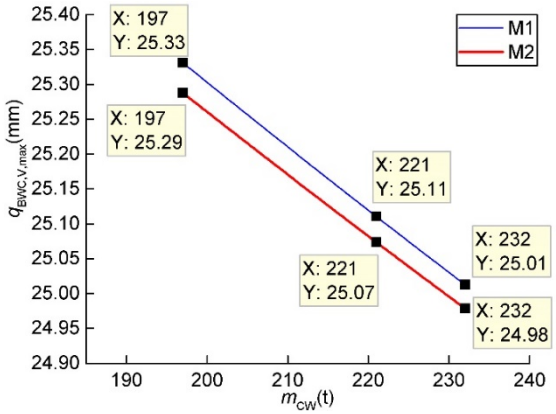

Fig. 15 Maximum vertical displacements of the BWC

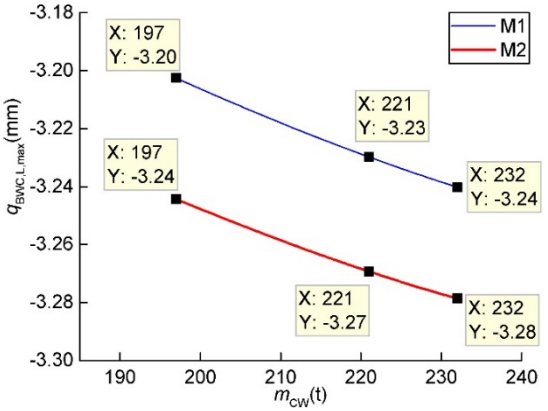

Fig. 16 Maximum lateral displacements of the BWC

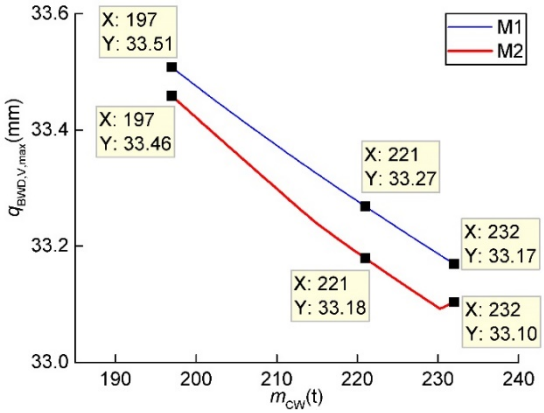

Fig. 17 Maximum vertical displacements of the BWD

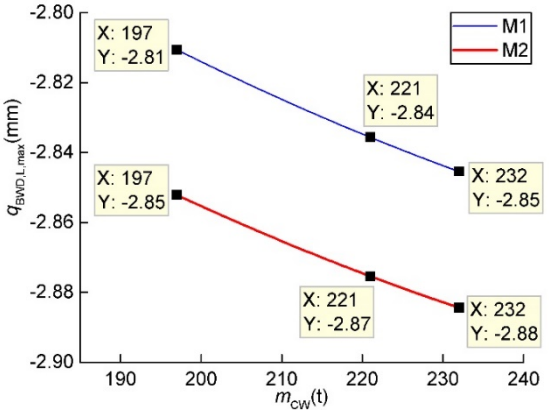

Fig. 18 Maximum lateral displacements of the BWD

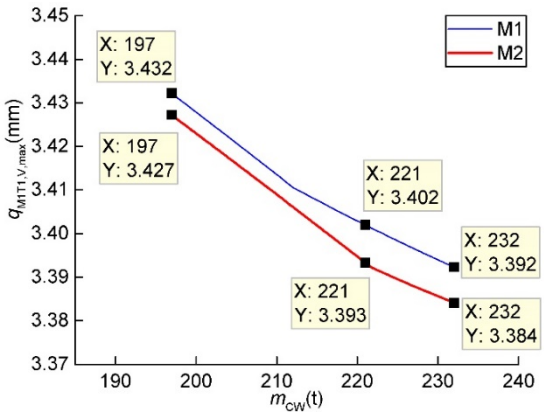

Fig. 19 Maximum vertical displacements of the M1T1

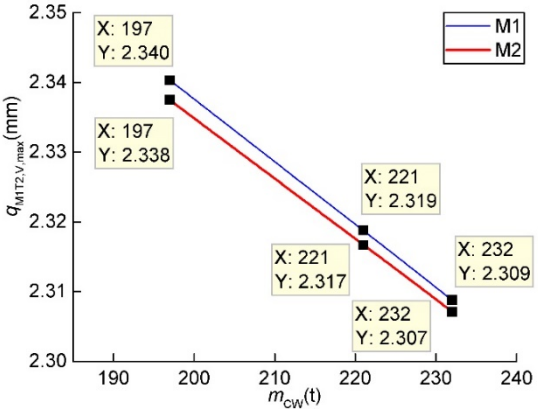

Fig. 20 Maximum vertical displacements of the M1T2

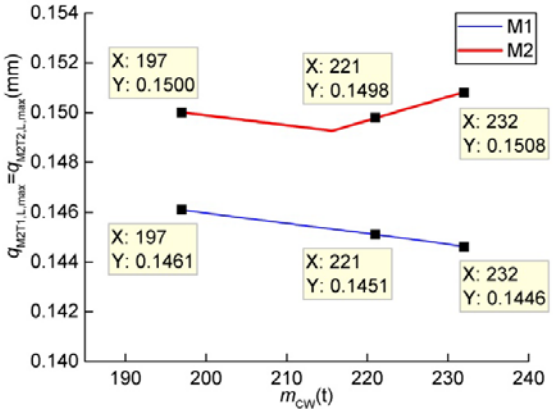

Fig. 24 Maximum lateral displacements of the M2T1 and M2T2

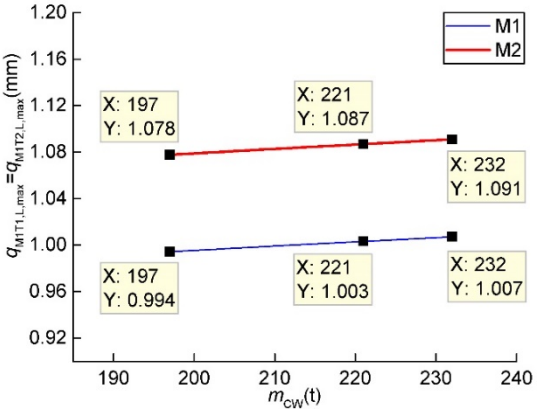

Fig. 21 Maximum lateral displacements of the M1T1 and M1T2

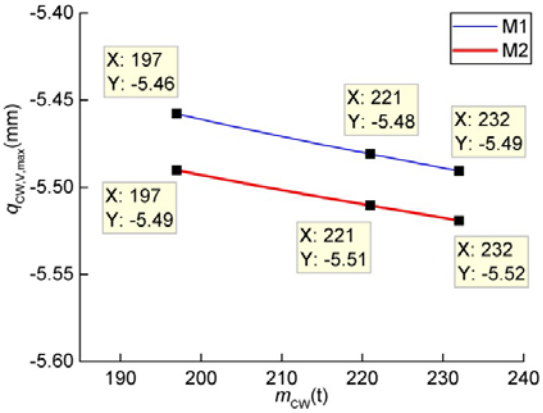

Fig. 25 Maximum vertical displacements of the CWC

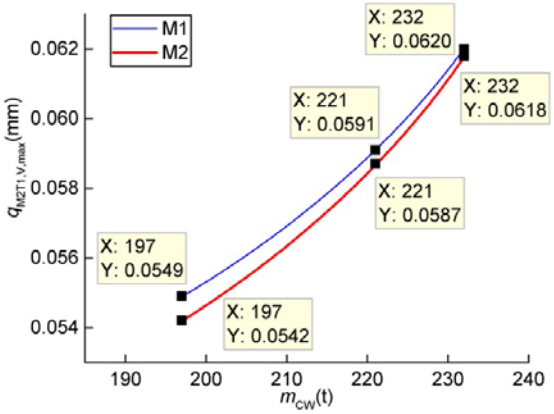

Fig. 22 Maximum vertical displacements of the M2T1

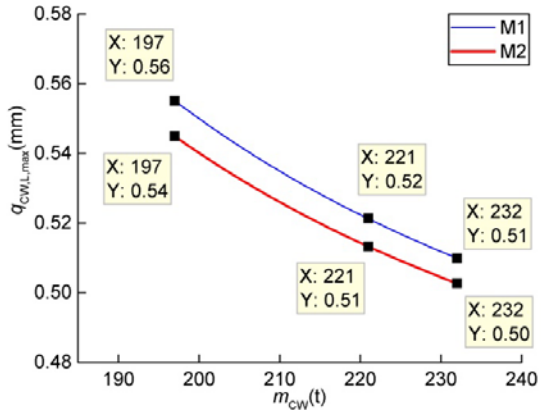

Fig. 26 Maximum lateral displacements of the CWC

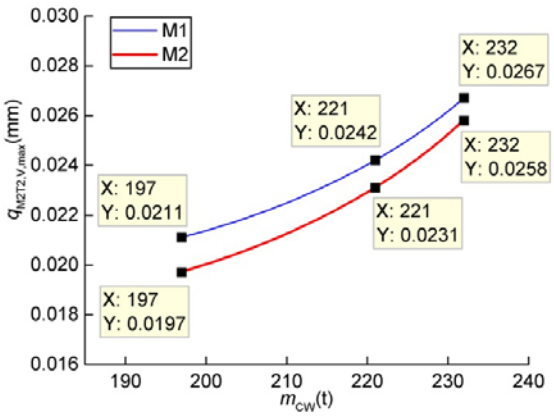

Fig. 23 Maximum vertical displacements of the M2T2

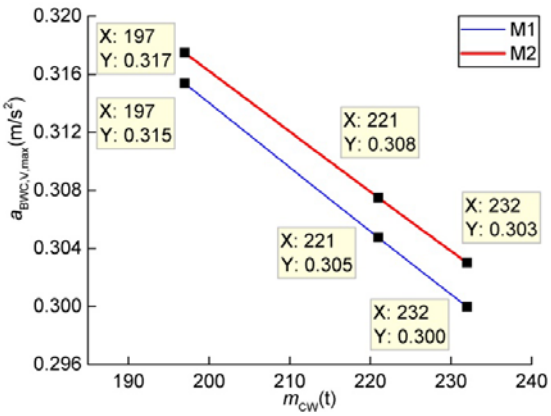

Fig. 27 Maximum vertical accelerations of the BWC

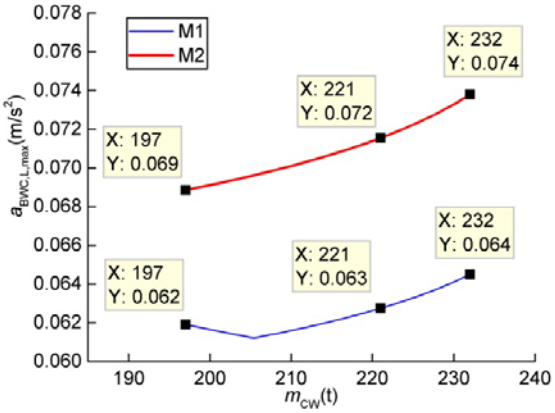

Fig. 28 Maximum lateral accelerations of the BWC

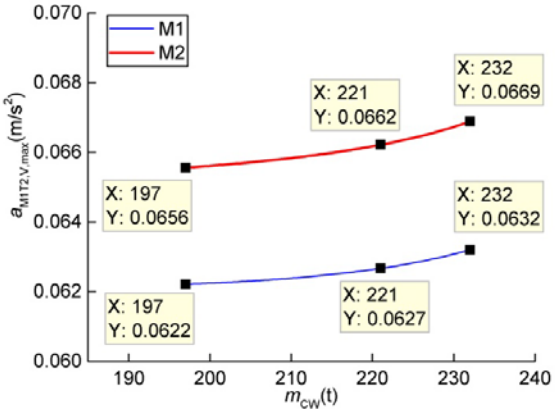

Fig. 32 Maximum vertical accelerations of the M1T2

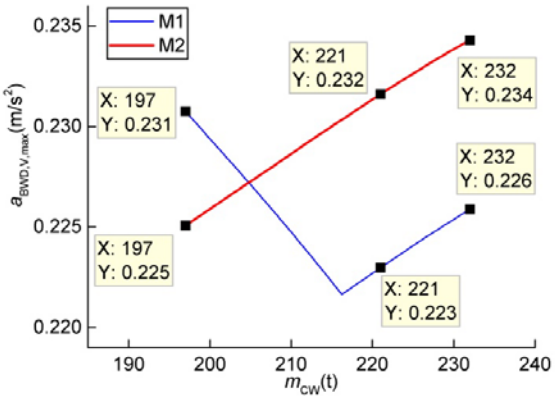

Fig. 29 Maximum vertical accelerations of the BWD

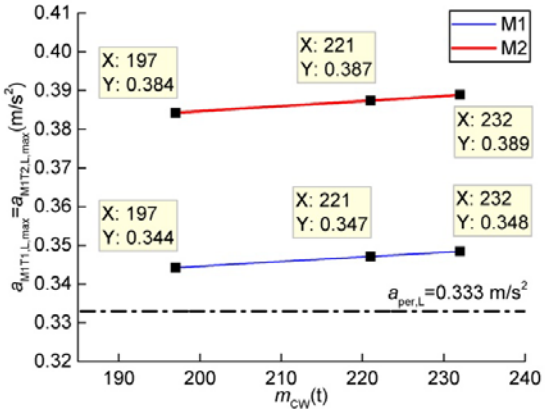

Fig. 33 Maximum lateral accelerations of the M1T1 and M1T2

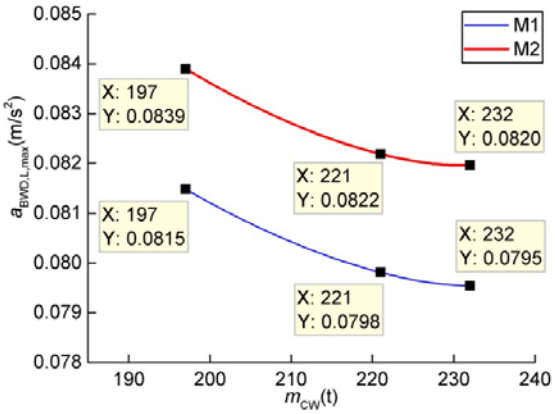

Fig. 30 Maximum lateral accelerations of the BWD

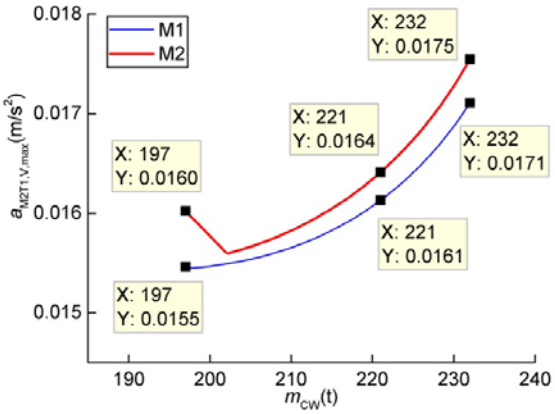

Fig. 34 Maximum vertical accelerations of the M2T1

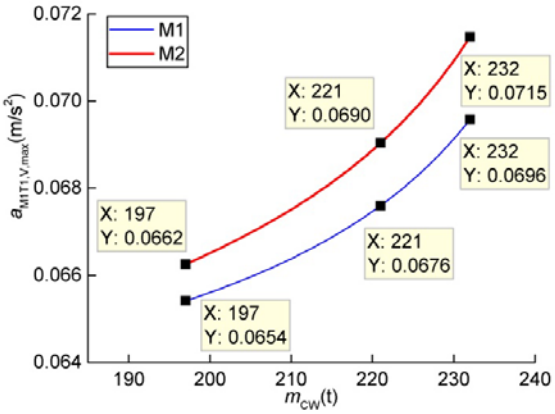

Fig. 31 Maximum vertical accelerations of the M1T1

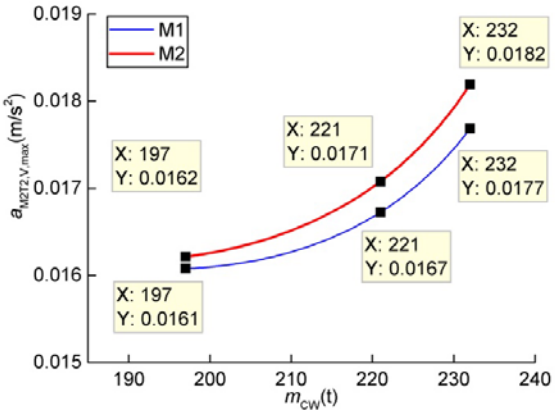

Fig. 35 Maximum vertical accelerations of the M2T2

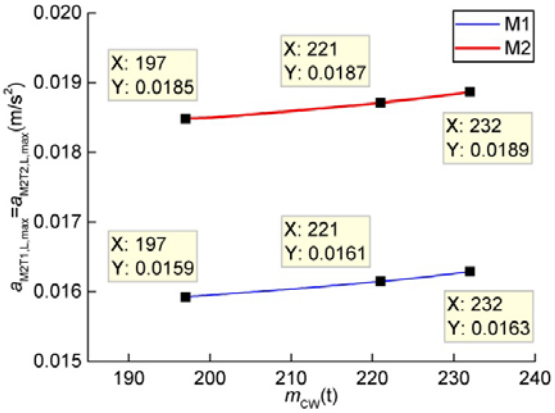

Fig. 36 Maximum lateral accelerations of the M2T1 and M2T2

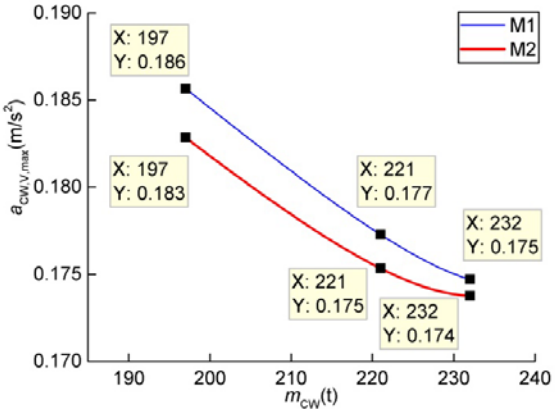

Fig. 37 Maximum vertical accelerations of the CWC

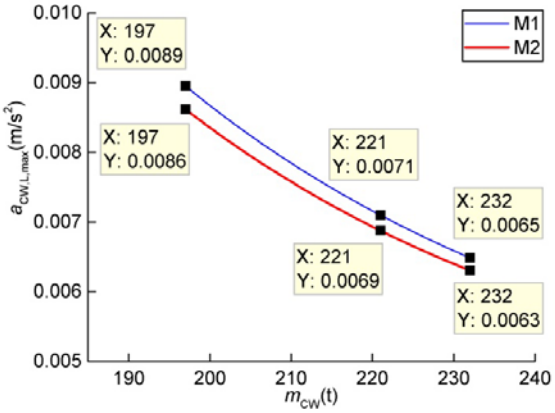

Fig. 38 Maximum lateral accelerations of the CWC

IV. Discussion

By harmonizing the mass of the 'a priori' model of the SS (model M1), Table I, and the mass of the SS, equation (1), determined by the results of the weighing W1, Table II, an 'a posteriori' model (model M2) of the SS has been formed. Its mass, Table V, is equal to the experimentally (W1) determined mass of the SS. Based on the values of the abscissas of the corrective mass, Table IV, it is concluded that excess mass of the model M2, in relation to the model M1, exists on the BWB.

Based on the comparative analysis of the results of the weighing W1, Table II, and the results obtained using the models M1 and M2, Tables III and V, the following conclusions are drawn: (1) the CoG abscissas of the model M1 deviate considerably from the experimentally determined SS CoG abscissas, Fig. 5, Table IX: the lowest absolute value of deviation occurs at the high position of the BWB and equals to 260 mm, and the highest, which is 323 mm, occurs at the low position of the BWB; (2) the CoG abscissas of the model M2 are in good accordance with the experimentally determined SS CoG abscissas, Table IX: the lowest absolute value of deviation occurs at the horizontal BWB position and, with the adopted level of precision equals to 0, and the highest, which is 6 mm, occurs at the high position of the BWB; (3) ordinate deviations are within acceptable ranges for both models, whereby said deviations are considerably lower in the case of model M2, Table IX. In control weighing W2 (CW mass $m_{CW,E}$=231.977 t) the deviations of CoG abscissas of the models M1 and M2 from the experimentally determined SS CoG abscissa, Fig. 7, equal to 367 mm and 45 mm, respectively. The increase of the considered deviations from the deviations in weighing W1 is dominantly the consequence of the presence of foreign bodies (≈1.24 t) and snow accumulation [44].

TABLE IX CoG Position: W1 vs. Models M1 and M2

BWB measuring position	Deviation (mm)			
	Δx_{CoG}*		Δy_{CoG}**	
	M1	M2	M1	M2
Low (L): α_{BWB}=–12.9°	–323	–5	9	0
Horizontal (H): α_{BWB}=0	–290	0	5	–4
High (Hi): α_{BWB}=14.1	–260	–6	12	3

The differences of the CoG abscissas of the models M1 and M2 are positive and monotonously declining over the entire domain of change of the BWB inclination angle, Fig. 39. Additionally, it is observed that the considered differences of abscissas rise as the mass of the counterweight increases, which is explained by the lower sensitivity of the BPSS of the M2 to the impact of the CW mass.

The corrective mass, i.e. the difference of the SS mass determined based on the results of weighing W1, equation (1), and its designed mass, Table I, equals to m_{cor}=16.98 t, equation (2), which represents

$$\Delta m_{SS,per} = 100\frac{m_{cor}}{m_{SS,0,M1}} = 100\frac{16.98}{978.266} = 1.7\%$$

of the designed mass of the SS. According to [15, page 233] "If the weighing results differ by more than a certain amount, in general 5% of the theoretical values calculated for stability, the calculation must be checked and the weighing procedure repeated. The ballast must then be adjusted according to the weighing results so that the position of the COG in the plane of the jacking points corresponds to the desired theoretical values.". Therefore, the provided quote, as well as the standard [50], imply that, having in mind the deviation of the designed and the SS mass determined by weighing is considerably lower than 5%, the correction of the ballast is not necessary. However, the results of the first weighing, conducted with the ballast mass of $m_{CW,W1}$=177.017 t, which is close to the mass of the ballast necessary for balancing of the SS deadweight: $m_{CW,0,H,F}$=177.5 t [41] i.e. $m_{CW,0,H,M1}$=179.263 t, Fig. 4, point to the significant impact of the corrective mass, which is the consequence of relatively high absolute values of its CoG abscissas, Table IV. For this reason it

was necessary to perform a correction to the designed ballast $m_{CW,D,F}$=221 t [41] (ballast CoG abscissa: x_{CW}=34.123 m) by adding

$$\Delta_1 m_{CW} = -\frac{m_{cor} x_{CMC,H}}{x_{CW}} = -\frac{16.98 \times (-20.09)}{34.123} = 9.997 \text{ t}.$$

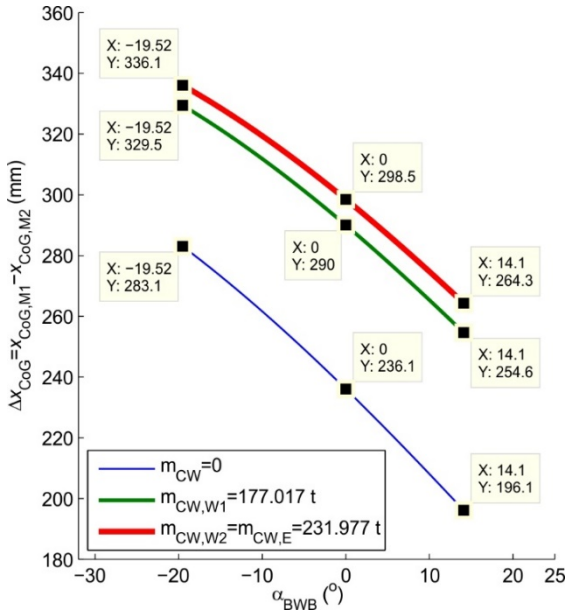

Fig. 39 Impact of the BWB angle on the difference of the SS models CoG abscissas

The higher mass of the BWB in the model M2 causes the increase in the intensity of forces in the ropes of the BWB hoisting mechanism, Fig. 6. The percent increment of the intensities of these forces, Fig. 40, monotonously decreases from 2.9% in the low position of the BWB, to 2.1% in its high position.

The differences of the CoG abscissas of the M1 and M2 SS models, for both referent positions of the BW, monotonously slowly rise as the mass of the CW increases, Fig. 41, which is the consequence of the mentioned lower sensitivity of the M2 BPSS to the influence of the CW mass. Additionally, it is observed that the mentioned differences are somewhat higher in the horizontal BWB position, which is explained by the higher impact of the corrective mass because of the greater distance of its center of mass from the RSB axis of rotation (*Oz*). The maximum values of abscissa differences $\Delta x_{CoG,H,max}$=299 mm and $\Delta x_{CoG,Hi,max}$=265 mm, Fig. 41, occur for the CW mass of $m_{CW,E}$=231.977 t with which the excavator was deployed. With this CW mass, the CoG abscissas of the designed SS (model M1) are $x_{CoG,H,M1}$=1486 mm and $x_{CoG,Hi,M1}$=2036 mm, Fig. 9, which means that the CoG abscissa of the deployed-state SS (M2) is lower by

$$100\frac{\Delta x_{CoG,H,max}}{x_{CoG,H,M1}} = 100\frac{299}{1486} = 20.1\%$$

in the horizontal position of the BWB, and

$$100\frac{\Delta x_{CoG,Hi,max}}{x_{CoG,Hi,M1}} = 100\frac{265}{2036} = 13.0\%$$

in the high BWB position.

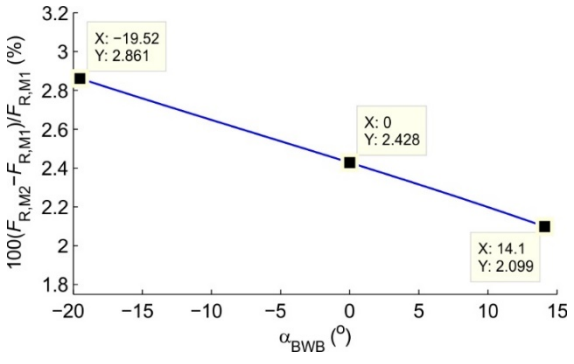

Fig. 40 Percentage difference of the winch rope forces

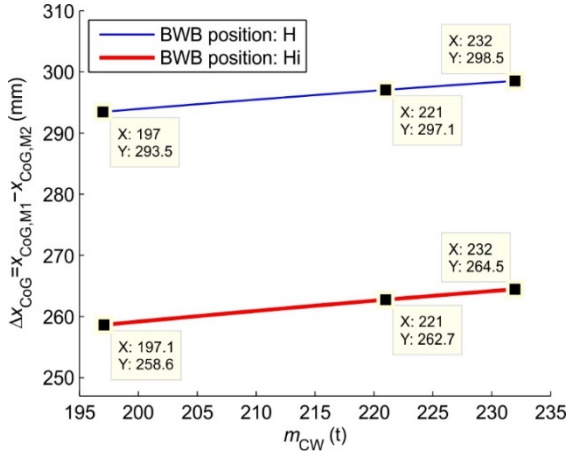

Fig. 41 Impact of the CW mass on the difference of the SS models CoG abscissas

A change in the CW mass significantly impacts the relative eccentricity of the vertical coordinate of the principal vector of loads on the RSB caused by main operating loads, Fig. 10. In the horizontal position of the BWB (BW side), the relative eccentricity monotonously decreases as the CW mass increases, Fig. 10(a), while in the high position of the BWB it is of a monotonously rising character, Fig. 10(b). Relative eccentricity of the load on the BW side in the model M2 does not satisfy the condition defined by the equation (3) for CW masses $m_{CW} \leq 204.3$ t. Fig. 10(a). In every other case, the relative eccentricities of the loads are lower than 0.25 for both SS models. It is observed, Fig. 10(a), that the relative eccentricity of loads on the BW side are higher in case of the model M2, while on the CW side it is higher in the model M1, Fig. 10(b). If the values of the relative eccentricities of loads for the model M1 are adopted as the basis for comparison, the percentage differences, Fig. 42, are of a monotonously rising character. At the CW mass $m_{CW,E}$=231.977 t, the relative eccentricity of the vertical load in the model M2 is 13.1% higher on the BW side and 11.5% lower on the CW side, Fig. 42. This means that the conditions for static stability of the SS of the model M2 are less favorable on the BW side and more favorable on the side of the CW.

A change in the mass of the SS and the relative eccentricity of the RSB load leads, naturally, to the change in the RSB ball maximum load, Fig. 11. The character of its dependence on the CW mass is the same as the character of dependence on the relative RSB vertical load eccentricity, Figs. 10 and 11. The same applies to the character of dependence of the percentage differences of the RSB ball maximum loads, Fig. 43. For

the CW mass of $m_{CW,E}$=231.977 t the maximum RSB ball load in the model M2 is 6.5% higher on the BW side and 3.9% lower on the CW side, Fig. 43.

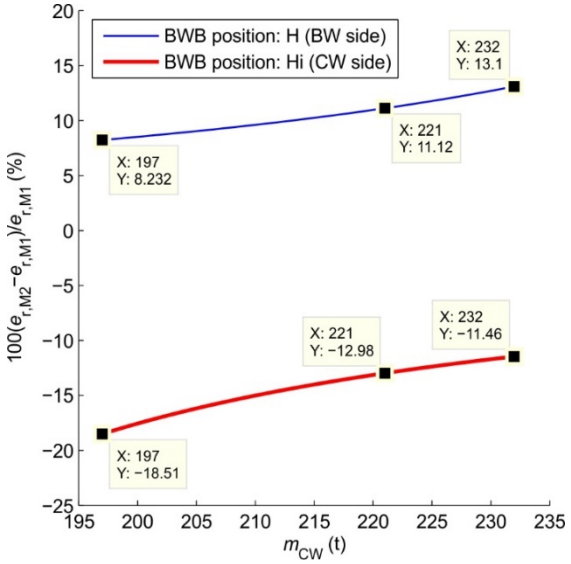

Fig. 42 Percentage difference of the relative eccentricity of the vertical RSB load

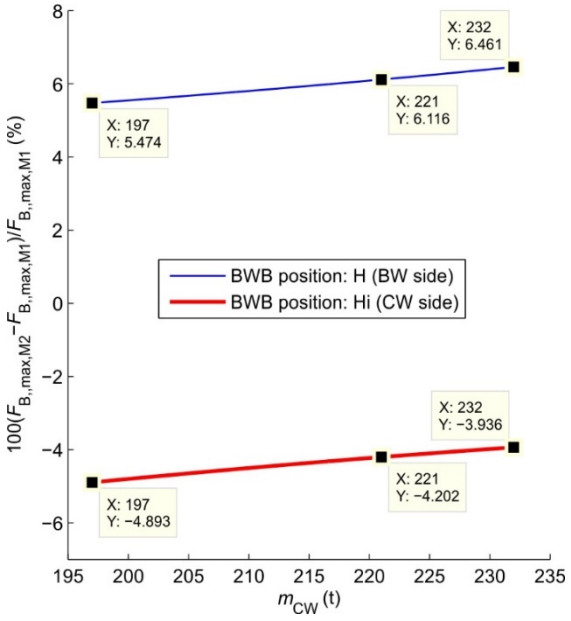

Fig. 43 Percentage difference of the RSB ball maximum load

The increase of both M1 and M2 models' masses has led, as expected, to the decrease in the values of their natural frequencies, Fig. 14 and Table VIII. The eleventh natural frequency of both models is the most affected by the increase of the CW mass, Table X. The second, third and fifth natural frequencies are declining by more than 2% in both of the analyzed models. The fundamental natural frequency of the model M1 is 1.5% lower when m_{CW}=$m_{CW,E}$ compared to the state of the model with m_{CW}=$m_{CW,D,P}$. For the same conditions, the fundamental, natural frequency of the model M2 is 1.4% lower, Table X. The decreases in the fourth, twelfth and thirteenth natural frequencies are lower than 1%, while the sixth through tenth natural frequencies are practically unaffected by the change in the CW mass for both of the analyzed models.

The transition from the 'a priori' image of the SS (model M1 with the mass of the CW $m_{CW,E}$) to the state in which the excavator was put in exploitation (model M2 with the CW mass $m_{CW,E}$) does not have any significant impact on the values of the natural frequencies, Table XI. The tenth and twelfth natural frequencies are 1.1% and 1.0% lower for the 'a posteriori' model, while all of the other analyzed natural frequencies are dropping by less than 1%, Table XI.

In the complete domain of CW mass change there is no appearance of resonances for neither of the analyzed models.

Maximum vertical displacements of the referent points which are influenced by the change in the CW mass the most are those of the tips of the mast 2 for both of the analyzed models, Table XII. Nevertheless, these displacements are an order of magnitude lower than the remainder of the analyzed displacements, Figs. 22 and 23, and are, for this reason, of no significance in further analysis. Maximum generalized vertical displacements of the referent points of the SS are influenced by the change of the CW mass in the domain from 0.5% to 1.3% for both of the analyzed models, drawing a conclusion that, from the engineering standpoint, this influence can be considered negligible, Table XII. Similar conclusions may be drawn when analyzing the influence of transition from the 'a priori' to the 'a posteriori' state of the SS where maximum vertical displacements of the BWD and M1T1 are 0.2% lower, followed by 0.1% lower displacements of the BWC and M1T2, Table XIII. Only the maximum vertical displacement of the CWC is higher, by 0.5%.

Maximum generalized lateral displacement most affected by the change of the CW mass is the displacement of the CWC, Fig. 26, which is 8.9% and 7.4% lower, respectively, at the end compared to the start of the analyzed interval of parameter change for models M1 and M2, Table XIV. The model M1 is slightly more affected by the change in the CW mass, Table XIV, although, from the engineering standpoint, this impact on the lateral displacements of other referent points can be considered negligible. On the other hand, the transition from the 'a priori' to the 'a posteriori' state of the SS has an impact on the lateral displacements of the referent points which may not be neglected steaming from the fact that M1T1 and M1T2 displacements are 8.3% higher, followed by 4.3%, 1.2% and 1.1% higher displacements of the tips of masts 2, BWC and BWD, Table XV. The maximum lateral displacement of the CWC is 2.0% lower.

Lateral displacements, Figs. 21 and 24, and accelerations, Figs. 33 and 36, of the tips of the mast 1 and the mast 2 are equal since these structures are symmetrical, symmetrically supported and symmetrically loaded constructions in the lateral direction.

All of the obtained maximum vertical accelerations of the SS referent points, for both of the analyzed models, are lower than permitted values prescribed by the code [46], Table XVI. Since the maximum obtained vertical accelerations of the tips of the masts 1 and 2, Figs. 31, 32, 34 and 35, are more than five times lower than the permitted values, Table XVI, these accelerations will not be discussed during further analysis. The reason behind the obtainment of the results of such low values lies in high axial stiffness of the cords of the analyzed masts (cords 5-8 in Fig. 12). Maximum vertical accelerations of

the CWC are the most affected by the variation of the CW mass. Vertical accelerations of this referent point are declining by 5.9% for model M1 and 6.5% for model M2, Fig. 37 and Table XVII. Maximum vertical accelerations of the BWC decline by 4.8% and 4.4%, with the increase of the CW mass for the models M1 and M2, respectively, Fig. 27 and Table XVII. This trend is also present in the maximum vertical accelerations of the BWD for the model M1 where a 2.2% decrease is observed, while these accelerations increase by 4% in case of the model M2. The character of the diagram of maximum vertical accelerations of the BWD for the model M1, Fig. 29, is the consequence of the fourth order resonant state, the influence of which was analyzed in [37].

Disregarding the percentage differences of the values of maximum vertical accelerations of the tips of the masts 1 and 2 for the already enclosed reasons, the transition from the 'a priori' to the 'a posteriori' state of the SS has the biggest effect on the vertical accelerations of the BWD, reflected in the increase of 3.5%, Table XVIII. The increase of values is also observed when analyzing the maximum vertical accelerations of the BWC (1.0%). Said transition has a slight positive influence only on the maximum vertical accelerations of the CWC, which decline by 0.6%, Table XVIII.

Having in mind the fact that the maximum lateral accelerations of the tips of the mast 2 (M2T1 and M2T2) and the CWC are by an order of magnitude lower than their permitted values, Table XVI, over the entire domain of the parameter change for both of the analyzed models it is conclusive that they are of no interest for further analysis, Figs. 36 and 38. With the increase in the CW mass, the values of the maximum lateral accelerations of the BWC increase by 3.2% and 7.2% for the models M1 and M2, respectively, Fig. 28, Table XIX. On the other hand, maximum lateral accelerations of the BWD decline by 2.5% (M1) and 2.3% (M2), Table XIX. The increase in the values of maximum lateral accelerations of the tips of the mast 1 with the increase of the CW mass is practically negligible (≤1.3%) for both of the analyzed models, Table XIX. However, unlike the maximum lateral accelerations of the BWC and the BWD, which are lower than the permitted value on the complete interval of the parameter change for both of the analyzed models, the values of the maximum lateral accelerations of the tips of the mast 1 are slightly higher (3.3% at the beginning and 4.5% at the end of the analyzed interval of change) than the permitted value for the model M1, Fig. 33 and Table XVI. Negative dynamic effects are even more pronounced when said accelerations are analyzed for model M2, for which the values are higher by 15.3% and 16.8% for $m_{\mathrm{CW,D,P}}$ and $m_{\mathrm{CW,E}}$, than the permitted value prescribed by [46], respectively.

For the previously stated reasons, the influence of the transition from the 'a priori' to the 'a posteriori' state of the SS on the maximum lateral accelerations of the tips of the mast 2 and the CWC was not analyzed. Said transition has a significant impact on the values of maximum lateral accelerations of the BWC (increase of 15.6%) and the tips of the mast 1 (increase of 11.8%), while the BWD is slightly less affected (increase of 3.1%), Table XX. Finally, the values of maximum lateral accelerations of the tips of the mast 1 are only 4.5% higher than the permitted value when the 'a priori' state of the SS is analyzed, compared to 16.8% higher values obtained for the state of the SS that was put in exploitation.

TABLE X PERCENTAGE DECREASE OF M1 AND M2 NATURAL FREQUENCIES CAUSED BY CW MASS INCREASE

Model	**Percentage difference**	**Natural frequency (i=1,2...13)**												
		f_1	f_2	f_3	f_4	f_5	f_6	f_7	f_8	f_9	f_{10}	f_{11}	f_{12}	f_{13}
M1	$\frac{f_i^{m_{\mathrm{CW,E}}} - f_i^{m_{\mathrm{CW,D,P}}}}{f_i^{m_{\mathrm{CW,D,P}}}} \times 100$	-1.5	-2.2	-2.6	-0.9	-2.3	0.0	0.0	0.0	0.0	0.0	-3.3	-0.7	-0.2
M2		-1.4	-2.0	-2.7	-0.8	-2.3	0.0	0.0	0.0	0.0	0.0	-3.2	-0.9	-0.3

TABLE XI TRANSITION FROM THE 'A PRIORI' TO THE 'A POSTERIORI' STATE OF THE SS - IMPACT ON THE SPECTRUM OF NATURAL FREQUENCIES

Percentage difference	**Natural frequency (i=1,2...13)**												
	f_1	f_2	f_3	f_4	f_5	f_6	f_7	f_8	f_9	f_{10}	f_{11}	f_{12}	f_{13}
$\frac{f_i^{\mathrm{M2}(m_{\mathrm{CW,E}})} - f_i^{\mathrm{M1}(m_{\mathrm{CW,E}})}}{f_i^{\mathrm{M1}(m_{\mathrm{CW,E}})}} \times 100$	-0.4	-0.2	-0.3	-0.4	-0.4	-0.1	-0.1	0.0	-0.1	-1.0	-0.2	-1.1	-0.7

TABLE XII DEVIATION OF MAXIMUM GENERALIZED VERTICAL DISPLACEMENTS CAUSED BY CW MASS INCREASE

Model	**Percentage difference**	**Referent point (RP)**						
		BWC	BWD	M1T1	M1T2	M2T1	M2T2	CWC
M1	$\frac{q_{RP,\mathrm{V,max}}^{m_{\mathrm{CW,E}}} - q_{RP,\mathrm{V,max}}^{m_{\mathrm{CW,D,P}}}}{q_{RP,\mathrm{V,max}}^{m_{\mathrm{CW,D,P}}}} \times 100$	-1.3	-1.0	-1.2	-1.3	12.9	26.5	0.5
M2		-1.2	-1.1	-1.3	-1.3	14.0	31.0	0.5

TABLE XIII TRANSITION FROM THE 'A PRIORI' TO THE 'A POSTERIORI' STATE OF THE SS - IMPACT ON THE MAXIMUM VERTICAL DISPLACEMENTS

Percentage difference	**Referent point (RP)**						
	BWC	BWD	M1T1	M1T2	M2T1	M2T2	CWC
$\frac{q_{RP,\mathrm{V,max}}^{\mathrm{M2}(m_{\mathrm{CW,E}})} - q_{RP,\mathrm{V,max}}^{\mathrm{M1}(m_{\mathrm{CW,E}})}}{q_{RP,\mathrm{V,max}}^{\mathrm{M1}(m_{\mathrm{CW,E}})}} \times 100$	-0.1	-0.2	-0.2	-0.1	-0.3	-3.4	0.5

TABLE XIV DEVIATION OF MAXIMUM GENERALIZED LATERAL DISPLACEMENTS CAUSED BY CW MASS INCREASE

Model	Percentage difference	Referent point (*RP*)				
		BWC	BWD	M1T1; M1T2	M2T1; M2T2	CWC
M1	$\frac{q_{RP,\mathrm{L},\max}^{m_{\mathrm{CW,E}}} - q_{RP,\mathrm{L},\max}^{m_{\mathrm{CW,D,P}}}}{q_{RP,\mathrm{L},\max}^{m_{\mathrm{CW,D,P}}}} \times 100$	1.3	1.4	1.3	-1.0	-8.9
M2		1.2	1.1	1.2	0.5	-7.4

TABLE XV TRANSITION FROM THE 'A PRIORI' TO THE 'A POSTERIORI' STATE OF THE SS - IMPACT ON THE MAXIMUM LATERAL DISPLACEMENTS

Percentage difference	Referent point (*RP*)				
	BWC	BWD	M1T1; M1T2	M2T1; M2T2	CWC
$\frac{q_{RP,\mathrm{L},\max}^{\mathrm{M2}(m_{\mathrm{CW,E}})} - q_{RP,\mathrm{L},\max}^{\mathrm{M1}(m_{\mathrm{CW,E}})}}{q_{RP,\mathrm{L},\max}^{\mathrm{M1}(m_{\mathrm{CW,E}})}} \times 100$	1.2	1.1	8.3	4.3	-2.0

TABLE XVI PERMITTED ACCELERATION VALUES ACCORDING TO THE STANDARD [46]

Permitted acceleration (m/s^2)	Referent point (*RP*)	
	BWC; BWD	M1T1; M1T2; M2T1; M2T2; CWC
Vertical direction	1	0.4
Lateral direction	0.167	0.333

TABLE XVII DEVIATION OF MAXIMUM GENERALIZED VERTICAL ACCELERATIONS CAUSED BY CW MASS INCREASE

Model	Percentage difference	Referent point (*RP*)						
		BWC	BWD	M1T1	M1T2	M2T1	M2T2	CWC
M1	$\frac{a_{RP,\mathrm{V},\max}^{m_{\mathrm{CW,E}}} - a_{RP,\mathrm{V},\max}^{m_{\mathrm{CW,D,P}}}}{a_{RP,\mathrm{V},\max}^{m_{\mathrm{CW,D,P}}}} \times 100$	-4.8	-2.2	6.4	1.6	10.3	9.9	-5.9
M2		-4.4	4.0	8.0	2.0	9.4	12.3	-6.5

TABLE XVIII TRANSITION FROM THE 'A PRIORI' TO THE 'A POSTERIORI' STATE OF THE SS - IMPACT ON THE MAXIMUM VERTICAL ACCELERATIONS

Percentage difference	Referent point (*RP*)						
	BWC	BWD	M1T1	M1T2	M2T1	M2T2	CWC
$\frac{a_{RP,\mathrm{V},\max}^{\mathrm{M2}(m_{\mathrm{CW,E}})} - a_{RP,\mathrm{V},\max}^{\mathrm{M1}(m_{\mathrm{CW,E}})}}{a_{RP,\mathrm{V},\max}^{\mathrm{M1}(m_{\mathrm{CW,E}})}} \times 100$	1.0	3.5	2.7	5.9	2.3	2.8	-0.6

TABLE XIX DEVIATION OF MAXIMUM GENERALIZED LATERAL ACCELERATIONS CAUSED BY CW MASS INCREASE

Model	Percentage difference	Referent point (*RP*)				
		BWC	BWD	M1T1; M1T2	M2T1; M2T2	CWC
M1	$\frac{a_{RP,\mathrm{L},\max}^{m_{\mathrm{CW,E}}} - a_{RP,\mathrm{L},\max}^{m_{\mathrm{CW,D,P}}}}{a_{RP,\mathrm{L},\max}^{m_{\mathrm{CW,D,P}}}} \times 100$	3.2	-2.5	1.2	2.5	-27.0
M2		7.2	-2.3	1.3	2.2	-26.7

TABLE XX TRANSITION FROM THE 'A PRIORI' TO THE 'A POSTERIORI' STATE OF THE SS - IMPACT ON THE MAXIMUM LATERAL ACCELERATIONS

Percentage difference	Referent point (*RP*)				
	BWC	BWD	M1T1; M1T2	M2T1; M2T2	CWC
$\frac{a_{RP,\mathrm{L},\max}^{\mathrm{M2}(m_{\mathrm{CW,E}})} - a_{RP,\mathrm{L},\max}^{\mathrm{M1}(m_{\mathrm{CW,E}})}}{a_{RP,\mathrm{L},\max}^{\mathrm{M1}(m_{\mathrm{CW,E}})}} \times 100$	15.6	3.1	11.8	16.0	-3.1

V. CONCLUSIONS

Balancing of the BWE SS represents the final stage of the excavator's production. Conducted upon the conclusion of the first erection and before the excavator undergoes the proof of capacity and the test run, the outcome of this procedure significantly affects the exploitation behavior and the lifespan of the vital elements of the machine.

The basis for the balancing of the SS lies in the results of the experimental determination of its weight and CoG position. In the referent literature [15] and technical regulations [50] it is stated that the adjustment of the ballast is to be conducted if the obtained weight of the SS is more than 5% higher than the analytically determined weight. Based on the results of the research presented in this paper it is concluded that a noticeably smaller difference (1.7%) between the experimentally and

analytically determined SS weights has a significant impact on the position of its CoG. Results of the weighing conducted with the analytically determined mass of the CW needed for the balancing of the SS deadweight have shown that the CoG abscissas of the realized SS are considerably lower than designed (‘a priori’ model of the SS): by 323 mm for the BWB in low measuring position, 290 mm for BWB in horizontal position and 260 mm for BWB in high position. Because of this, an ‘a posteriori’ model of the SS was developed based on the experimental results, whose mass matches the experimentally determined SS mass. Validation of this model, which simultaneously yields good approximations of the abscissa (maximum absolute deviation of 6 mm) and the ordinate (maximum absolute deviation of 4 mm), was performed on the basis of the results of two weighings. Results of the calculation indicate the following facts:

- over the entire domain of the BWB inclination angle, with the CW mass of m_{CW}=0, the CoG abscissas of the SS 'a posteriori' model are significantly lower (the biggest difference occurs in the high BWB position and equals 283 mm);
- over the entire domain of the BWB inclination angle, the difference of the CoG abscissas of the ‘a priori’ and ‘a posteriori’ models of the SS rises with the increase in the CW mass;
- the biggest percentage increment in the intensity of the forces in the ropes of the BWB hoisting mechanism in the 'a posteriori' model of the SS, caused by the increased deadweight of the SS (excess mass compared to the 'a priori' model exists on the BWB substructure), equals 2.9% and occurs in the its low position;

Based on the comparative analysis of the results obtained from the 'a priori' and 'a posteriori' models of the SS, with the CW mass of $m_{CW,E}$=231.977 t, with which the excavator was deployed, the following has been concluded:

- the CoG abscissa of the 'a posteriori' SS model in the horizontal BWB position, which is relevant for the proof of stability on the BW side, is 20.1% lower, meaning that in that case the results of the static stability calculations for the 'a priori' model are not on the side of safety;
- the CoG abscissa of the 'a posteriori' SS model in the high BWB position, which is relevant for the proof of stability on the CW side, is 13.0% lower, meaning that in that case the results of the static stability calculations for the 'a priori' model are on the side of safety;
- the relative eccentricity of the vertical load on the RSB caused by the main operating loads in the 'a posteriori' SS model are 13.1% higher on the BW side and 11.5% lower on the CW side;
- the maximum RSB ball load in the 'a posteriori' SS model is 6.5% higher on the BW side and 3.9% lower on the CW side;
- the transition from the ‘a priori’ image of the SS to the state in which the excavator was put in exploitation does not have any significant impact on the values of the natural frequencies. The tenth and the twelfth natural frequencies are 1.1% and 1.0% lower, respectively, for the ‘a posteriori’ model, while all the other analyzed natural frequencies are dropping by less than 1%;
- similar conclusions may be drawn when analyzing the influence of the said transition on the maximum vertical displacements of the system referent points, where the highest deviation of the maximum vertical displacement is observed for the CWC (a rise of 0.5%);
- on the other hand, the influence of the transition from the ‘a priori’ to the ‘a posteriori’ state of the SS has an impact on the lateral displacements of the referent points which cannot be neglected, stemming from the fact that the displacements of the M1T1 and M1T2 are 8.3% higher, followed by 4.3%, 1.2% and 1.1% higher displacements of the tips of the mast 2, BWC and BWD. The maximum lateral displacement of the CWC is 2.0% lower;
- the transition from the ‘a priori’ to the ‘a posteriori’ state of the SS has the most significant effect on the vertical accelerations of the BWD, reflected on the increase by 3.5%;
- said transition has a significant negative impact on the values of maximum lateral accelerations of the BWC (increase of 15.6%) and the tips of the mast 1 (increase of 11.8%), while the BWD is slightly less affected (increase of 3.1%);
- finally, the values of maximum lateral accelerations of the tips of the mast 1 are 4.5% higher than the permitted value when the ‘a priori’ state of the SS is analyzed. Negative dynamic effects are even more pronounced for the state of the SS put in exploitation, where 16.8% higher values of the analyzed maximum accelerations are obtained.

Based on the presented, it is concluded that, upon the experimental determination of the mass and the CoG position of the SS, even in case of deviations lower than 5% to that of the designed state, it is necessary to analyze the levels of impact of the determined differences on the: (1) static stability; (2) intensities of forces in the ropes of the BWB hoisting mechanism; (3) maximum RSB ball loads; (4) dynamic response of the SS. Finally, having in mind the variety of design conceptions, dimensions and masses of the SSs in BWEs, the results of the presented research on the level of impact of the unharmonized designed and realized states cannot be generalized, but point to the necessity to form a consistent methodology for harmonizing the calculation models with the realized states of BWE SSs. In addition to BWEs, such a methodology could successfully be applied to bucket wheel reclaimers and spreaders.

ACKNOWLEDGMENT

This work is a contribution to the Ministry of Education, Science and Technological Development of Serbia funded project "Integrated research in the fields of macro, micro and nano mechanical engineering" (Contract number: 451-03-68/2020-14/200105).

The authors would like to express their gratitude to the ITO Foundation and The Joint Japan-Serbia Center for the Promotion of Science and Technology for providing the resources to conduct simulations.

REFERENCES

[1] Coal industry across Europe, 7th ed. Brussels: EURACOAL AISBL - European Association for Coal and Lignite, 2020.

[2] Production of electricity. Belgrade: Electric Power Industry of Serbia (EPS), http://www.eps.rs/eng/Poslovanje-EE.

[3] Energy sector development strategy of the Republic of Serbia for the period by 2025 with projections by 2030. Belgrade: Ministry of Mining and Energy, 2016.

[4] H. Hartman and J. Mutmansky, Introductory mining engineering, 2nd ed. Hoboken, New Jersey: John Wiley & Sons, 2002.

[5] M. Pantelić, S. Bošnjak, M. Misita, N. Gnjatović, and A. Stefanović, "Service FMECA of a bucket wheel excavator", Eng. Fail Anal., Vol. 108, article number104289, 2020.

[6] B. Schlecht, Investigation and optimization of the dynamic behavior of bucket wheel drives (Final report of the research project 16575 BR funded by the Federal Ministry for Economic Affairs and Energy of Germany). Dresden: Technische Universität IMM, 2014.

[7] E. Rusiński, J. Czmochowski, P. Moczko and D. Pietrusiak, Surface Mining Machines - Problems of Maintenance and Modernization. Cham: Springer International Publishing AG, 2017.

[8] S. Bošnjak, Z. Petković, N. Zrnić and S. Petrić, "Mathematical modeling of dynamic processes of bucket wheel excavators", in Proceedings of the 5th MATHMOD. Vienna: ARGESIM–Verlag, 2006, pp. 4.1-4.10.

[9] S. Bošnjak, N. Zrnić and Z. Petković, "Bucket wheel excavators and trenchers–computer added calculation of loads caused by resistance to excavation", in Machine Design, S. Kuzmanović, Ed. Novi Sad: University of Novi Sad, 2008, pp. 121-128.

[10] S. Bošnjak, Z. Petković, N. Zrnić, G. Simić, and A. Simonović, "Cracks, repair and reconstruction of bucket wheel excavator slewing platform", Eng. Fail Anal., Vol. 16, Issue 5, pp. 1631-1642, 2009.

[11] S. Bošnjak, N. Zrnić, V. Gašić, Z. Petković and A. Simonović, "External load variability of multibucket machines for mechanization", Adv. Mater. Res., Vol. 422, pp. 678-683, 2012.

[12] S. Bošnjak, M. Arsić, N. Zrnić, M. Rakin and M. Pantelić, "Bucket wheel excavator: Integrity assessment of the bucket wheel boom tie-rod welded joint", Eng. Fail. Anal., Vol 18, Issue 1, pp. 212-222, 2011.

[13] S. Bošnjak, M. Arsić, S. Savićević, G. Milojević and D. Arsić, "Fracture analysis of the pulley of a bucket wheel boom hoist system", Eksploat. Niezawodn., Vol 18, No. 2, pp. 155-163, 2016.

[14] S. Bošnjak, N. Gnjatović, S. Savićević, M. Pantelić and I. Milenović, "Basic parameters of the static stability, loads and strengthof the vital parts of a bucket wheel excavator's slewing superstructure", J. Zhejiang. Univ.-Sc. A, Vol. 17, Issue 5, pp. 353-365, 2016.

[15] W. Durst and W. Vogt, Bucket Wheel Excavator. Clausthal-Zellerfeld: Trans Tech Publications, 1988.

[16] D. Dudek, "Experimentelle Ermittlung der Stabilitat von Maschinen auf Schienenfahrwerken", Fördern und Heben, Vol. 40, No. 8, pp. 546-548, 1990.

[17] P. Maslak, G. Przybylek and T. Smolnicki, "Comparison of selected methods for the determination of the center of gravity in surface mining machines", in Materials Today: Proceedings, Vol. 4, No. 5 (part 1), pp. 5877-5882, 2017.

[18] N. Nan, I. Kovacs, I. and F. Popescu, "Balance control by weighting and tensiometric measurements of bucket wheel excavators", in WSEAS Transactions on Systems and Control, Vol. 3, No. 11, pp. 927-938, 2008.

[19] T. Smolnicki and M. Stańco, "Determination of Centre of Gravity of Machines with the Rail Undercarriage", Sol. St. Phen., Vol. 165, pp. 359-364, 2010.

[20] T. Smolnicki, M. Stańco and D. Pietrusiak, "Distribution of loads in the large size bearing – problems of identification", Teh. Vjesn., Vol. 20, No. 5, pp. 831-836, 2013.

[21] T. Smolnicki, G. Pękalski, J. Jakubik and P. Harnatkiewicz, "Investigation into wear mechanisms of the bearing raceway used in bucket wheel excavators", Arch. Civ. Mech. Eng., Vol. 17, Issue 1, pp. 1-8, 2017.

[22] P. Jovančić, D. Ignjatović, M. Tanasijević and T. Maneski, "Load-bearing steel structure diagnostics on bucket wheel excavator, for the purpose of failure prevention", Eng. Fail. Anal., Vol. 18, Issue 4, pp. 1203-1211, 2011.

[23] S. Bošnjak, N. Zrnić, D. Momčilović, N. Gnjatović and I. Milenović, "Tie-rods of the Bucket Wheel Excavator Slewing Superstructure: A Study of the Eye Plate Stress State", Eng. Struct., Vol. 207, article number 110233, 2020.

[24] E. Rusiński, S. Dragan, P. Moczko and D. Pietrusiak, "Implementation of experimental method of determining modal characteristics of surface mining machinery in the modernization of the excavating unit", Arch. Civ. Mech. Eng., Vol.12, Issue 4, pp. 471-476, 2012.

[25] D. Pietrusiak, P. Moczko and E. Rusiński, "Recent achievements in investigations of dynamics of surface mining heavy machines", in Proceedings of the 24th World Mining Congress. Rio de Janeiro: IBRAM, 2016, pp. 295-308.

[26] D. Pietrusiak, "Evaluation of large-scale load-carrying structures of machines with the application of the dynamic effects factor", Eksploat. Niezawodn., Vol. 19, No. 4, pp. 542-551, 2017.

[27] D. Pietrusiak, P. Moczko and E. Rusiński, "World's largest movable mining machine vibration testing - numerical and experimental approach", in Proceedings of International Conference on Noise and Vibration Engineering (ISMA2016) and International Conference on Uncertainty in Structural Dynamics (USD2016). Leuven: Katholieke Universitet Leuven,2016, pp. 2287–2299.

[28] P. Moczko and D. Pietrusiak, "Experimental–numerical method for assessing the condition of opencast mining and material handling equipment", Aust. J. Struct. Eng., vol. 20, issue 4, pp. 248-258, 2019.

[29] P. Moczko, D. Pietrusiak and E. Rusiński, "Material handling and mining equipment - International standards, recommendations for design and testing", FME Trans., Vol. 46, No. 3, pp. 291-298, 2018.

[30] P. Jovančić, D. Ignjatović, T. Maneski, D. Novaković and Č. Slavković, "Diagnostic procedure of bucket wheel and boom computer modeling – A case study: Revitalization bucket wheel and drive of BWE SRs 2000", in Proceedings of the 14th International Scientific Conference: Computer Aided Engineering. CAE 2018, Lecture Notes in Mechanical Engineering, E. Rusiński and D. Pietrusiak, Eds. Cham: Springer, pp. 310-318, 2019.

[31] A. Brkić, T. Maneski, D. Ignjatović, P. Jovančić and V. Spasojević Brkić, "Diagnostics of bucket wheel excavator discharge boom dynamic performance and its

reconstruction", Eksploat. Niezawodn., Vol. 16, No. 2, pp. 188-197, 2014.

[32] J. Gottvald, "The calculation and measurement of the natural frequencies of the bucket wheel excavator SchRs 1320/4x30", Transport, Vol. 25, No. 3, pp. 269-277, 2010.

[33] S. Bošnjak, N. Gnjatović and I. Milenović, "From 'a priori' to 'a posteriori' static stability of the slewing superstructure of a bucket wheel excavator", Eksploat. Niezawodn.,
Vol. 20, No. 2, pp. 190-206, 2018.

[34] N. Gnjatović, S. Bošnjak and N. Zrnić, "Spatial Reduced Dynamic Model of a Bucket Wheel Excavator with Two Masts", in Proceedings of the 14th International Scientific Conference: Computer Aided Engineering. CAE 2018, Lecture Notes in Mechanical Engineering, E. Rusiński and D. Pietrusiak, Eds. Cham: Springer, pp. 215-235, 2019.

[35] S. Bošnjak, D. Oguamanam and N. Zrnić, "On the dynamic modeling of bucket wheel excavators", FME Trans.,
Vol. 34, No. 4, pp. 221-226, 2006.

[36] S. Bošnjak and N. Gnjatović, "The influence of geometric configuration on response of the bucket wheel excavator superstructure", FME Trans., Vol. 44, No. 3, pp. 313-323, 2016.

[37] N. Gnjatović, S. Bošnjak and A. Stefanović, "The dependency of the dynamic response of a two mast bucket wheel excavator superstructure on the counterweight mass and the degree of Fourier approximation of the digging resistance", Arch. Min. Sci., Vol. 63, No. 2, pp. 491-509, 2018.

[38] N. Gnjatović, S. Bošnjak and I. Milenović, "The influence of incrustation and chute blockage on the dynamic behaviour of a bucket wheel excavator slewing superstructure", J. Theor. Appl. Mech., Vol. 58, No. 3, pp. 573-584, 2020.

[39] S. Bošnjak, D. Oguamanam and N. Zrnić, "The influence of constructive parameters on response of bucket wheel excavator superstructure in the out-of-resonance region", Arch. Civ. Mech. Eng., Vol. 15, Issue 4, pp. 977-985, 2015.

[40] S. Bošnjak, N. Gnjatović, Z. Petković, I. Milenović and A. Stefanović, "Determination of the static stability parameters of the superstructure of the bucket wheel excavator SchRs 1600 deployed in the open pit mine Tamnava West Field", comissioned by the Mining Basin "Kolubara", Belgrade: University of Belgrade-Faculty of Mechanical Engineering, 2015.

[41] BWE SchRs 1600: Final stability calculation-Rev 1. ThyssenKrupp Fördertechnik, 2009.

[42] BWE SchRs 1600: Weighing report No. 01/10. Vreoci: Kolubara-Metal, 2010.

[43] BWE SchRs 1600: Weighing. ThyssenKrupp Fördertechnik, 2010.

[44] BWE SchRs 1600: Weighing report No. 02/10. Vreoci: Kolubara-Metal, 2010.

[45] BWE SchRs 1600: Preliminary stability calculation-Rev 1. ThyssenKrupp Fördertechnik, 2007.

[46] DIN 22261-2: Excavators, spreaders and auxiliary equipment in opencast lignite mines – Part 2: Calculation principles. Berlin: Deutsches Institut für Normung, 2016.

[47] N. Gnjatović, S. Bošnjak, I. Milenović and A. Stefanović, "Bucket wheel excavators: Dynamic response as a criterion for validation of the total number of buckets", Eng. Struct., Article in Press, 2020.

[48] Rasper L. The Bucket Wheel Excavator Development Design Application. Clausthal-Zellerfeld: Trans Tech Publications; 1973.

[49] Volkov DP, Cherkasov VA. Dynamics and strength of multi-bucket excavators and stackers (in Russian). Moscow: Mašinostroenie; 1969.

[50] AS4324.1: Mobile equipment for continuous handling of bulk materials Part 1 - General requirements for the design of steel structures. Sydney: Standards Australia, 1995.